CIRCULATION COPY
SUBJECT TO RECALL
IN TWO WEEKS

UCRL- 84003
PREPRINT

ON THE MOTION FOLLOWING ISOCHORIC HEATING OF CONCENTRIC LIQUID ANNULI

L. A. Glenn

This paper was prepared for submittal to the International Journal of Nuclear Engineering and Design.

February 19, 1980

This is a preprint of a paper intended for publication in a journal or proceedings. Since changes may be made before publication, this preprint is made available with the understanding that it will not be cited or reproduced without the permission of the author.

Lawrence Livermore Laboratory

DISCLAIMER

This document was prepared as an account of work sponsored by an agency of the United States Government. Neither the United States Government nor the University of California nor any of their employees, makes any warranty, express or implied, or assumes any legal liability or responsibility for the accuracy, completeness, or usefulness of any information, apparatus, product, or process disclosed, or represents that its use would not infringe privately owned rights. Reference herein to any specific commercial product, process, or service by trade name, trademark, manufacturer, or otherwise, does not necessarily constitute or imply its endorsement, recommendation, or favoring by the United States Government or the University of California. The views and opinions of authors expressed herein do not necessarily state or reflect those of the United States Government or the University of California, and shall not be used for advertising or product endorsement purposes.

ON THE MOTION FOLLOWING ISOCHORIC HEATING OF CONCENTRIC LIQUID ANNULI*

L. A. Glenn
University of California, Lawrence Livermore Laboratory
Livermore, California 94550

ABSTRACT

When adjacent liquid slabs are separated by void gaps and suddenly heated throughout, each slab will split into two parts, which then move away from each other. If there are n initial gaps, there will eventually be at least $n(n+1)/2$ collisions. If the initial heating is non-uniform, the collisions will act to smear or average out the momentum generated within the fluid. Moreover, if the flow field is divergent, cavities will form in the liquid, the collisions will be inelastic, and energy will be dissipated. These phenomena were studied in connection with the design of an inertial confinement fusion reactor in which an array of concentric liquid lithium annuli, or close-packed jets, is suddenly penetrated by high-energy neutrons and simultaneously exposed to surface deposition of x-rays and ionic debris. It is shown that such a design can be very effective in reducing the outward-directed momentum and thus the impulse imparted to the reactor walls.

*Work performed under the auspices of the U.S. Department of Energy by Lawrence Livermore Laboratory under contract #W-7405-Eng-48.

1.0 INTRODUCTION

Liquids are almost never heated at constant volume in practice, except possibly within laboratory devices used to study their behavior at high pressures. And in this example, naturally enough, the bounding surfaces are rigid or quasi-rigid since the heating is accomplished rather slowly with a Bunsen burner or a resistance coil.

In inertial confinement fusion (ICF) however, rapid, isochoric heating of liquid lithium will very likely play a central role. The most likely ICF reactor construction has the deuterium-tritium (DT) fuel pellet surrounded by thick annuli[1)] or close-packed jets[2)] of lithium, whose function is: to breed tritium for pellet resupply, to act as an energy sink and heat exchange medium with an external power loop, and to protect the first wall from excessive neutronic and hydrodynamic loading. Most of the energy derived from the pellet is in the form of high energy (up to 14 MeV) neutrons for which the mean free path in lithium ranges up to 0.3 m[3)]. As a consequence, the liquid thickness must be 2-3 times this length to provide adequate moderation and to reduce the fluence on the first wall to an acceptable level[4)]. The energy release is virtually instantaneous when the DT pellet is imploded to the thermonuclear "burn" condition and the neutron penetration throughout the liquid occurs in a time period small in comparison with the time for release waves to move into the bulk of the fluid from any free surfaces. The liquid is therefore heated at constant volume, producing internal pressures as high as 1 GPa, although the average pressure from neutron heating will probably be lower by 1-2 orders of magnitude in a 1000 MW_e reactor (much higher pressures are produced by x-rays and ionic debris interaction, but only in a very thin liquid layer facing the pellet[1,2)]).

Early designs had the lithium injected as one continuous annular fall surrounding the pellet. Since the specific internal energy from the neutron deposition is typically 10-100 times higher at the inner radius than at the outer, this configuration tends to produce steep positive velocity gradients in the liquid. This is quite undesirable as it leads to high-speed spall layers and the first wall is then bombarded with potentially erosive drops or fragments. (Present designs call for a 1 Hz pulse rate and a 30 year operating life span so that of the order of 10^9 impacts are to be expected). The situation can be very much improved if the continuous annulus is replaced with a series of concentric annuli, separated by gaps. The reason is that the gaps allow pressure relief from surfaces which are interior to the main fall boundaries. This promotes momentum exchange between fluid elements moving in opposite directions and effectively smears or averages out the velocity distribution in the fall. (A further design improvement has been previously described[2] in which a close-packed annular array of jets is employed. This allows hot, high-pressure lithium plasma, deriving from the x-ray deposition and debris interaction, to vent from the cavity formed by the inner radius of the innermost annulus. The superposition of these concepts has also been discussed[5]).

When finite difference calculations were made of the disassembly and subsequent interaction of isochorically heated concentric liquid annuli, the results showed that, in addition to spacial averaging, the total momentum impinging on the first wall was reduced, implying that energy dissipation had occurred. Moreover, the dissipation increased as the gap(s) between the annuli were widened and as the number of gaps was increased. It is our main

purpose in what follows to describe this behavior in some detail and to explain why the dissipation occurs. The theory developed can also be applied to calculate the pressure exerted on the first wall by the impact of a cavitated fluid. This will be demonstrated for the case of a multi-annular lithium fall in a 1000 MW_e (2700 MJ) ICF reactor upon which the crossflow impulse (from the vented plasma) has been superposed.

2.0 TWO ANNULI SEPARATED BY A VOID GAP: THE MODEL

The problem is sketched in Figure 1. At time t = 0 two liquid annuli, each of thickness Δ, and separated by a void gap of width δ, are instantaneously heated. We assume, for the present, that the heating is uniform, so that the initial specific internal energy everywhere within the Lagrangian region $R_0 \leq r \leq R_1$ is e_0. Furthermore

$$e_0 << e_c \tag{1}$$

where e_c is the cohesive energy of the fluid, which in the case of lithium is 23.03 MJ/kg. We assume further that the equation of state (EOS) describing the slightly expanded liquid phase is of the Grüneisen form with a Clausius-Clapeyron-like term employed for the two-phase, liquid-vapor region[1]:

$$P = \text{Max} \begin{cases} \rho_0 C_0^2 (\eta - 1) + \gamma_0 \rho_0 e & \text{(2a)} \\ P_c \exp(1.4 - 1.481\, e_c/e) & \text{(2b)} \end{cases}$$

where ρ_0 is the reference liquid density, γ_0 is the Grüneisen parameter, C_0 is the sound speed at the melting point, and the constant P_c = 100 MPa. P, ρ, and e are respectively the pressure, density and specific internal energy, and $\eta = \rho/\rho_0$. For $\eta < 1 - \gamma_0 e/C_0^2$, the inequality (1) implies that $P \to 0$, i.e., the Clapeyron term in (2b) behaves like a tensile cut-off. In this case the EOS is similar to models used to describe porous materials[6]; as will be seen, the analogy is quite relevant.

Initially, $\eta = 1$ so that the pressure developed is $P_0 = \gamma_0 \rho_0 e_0$. The inner and outer radii of each annulus are free surfaces from which centered rarefactions then move into the fall interior. The free surface particle speed is

$$U_1 \approx P_0/\rho_0 C_0 = \gamma_0 e_0/C_0 \tag{3}$$

If we neglect the divergent geometry for the present, U_1 is also the speed along the trailing characteristic (tail of the expansion fan) which is itself moving at speed $C_0 - U_1$ into the fluid. Behind the tail, conditions are everywhere uniform and energy conservation requires the specific internal energy to have decreased to

$$e_1 = e_0 - \frac{1}{2} U_1^2 = e_0(1 - \gamma_0 M_0/2) \tag{4}$$

where we have defined the Mach number parameter

$$M_0 = \gamma_0 e_0/C_0^2 \tag{5}$$

The leading characteristic (head of the expansion fan) arrives at the center of each annulus at $t_0 \approx \Delta/2C_0$ and the pressure is reduced to zero everywhere shortly thereafter (although this may take up to twice as long when the spacial distribution of energy is initially non-uniform). The particle velocity distribution at this point will appear approximately as sketched in Figure 2. (In actuality, the interaction of the reflected characteristics at the center of the fall will create a nonsimple wave region which will result

in cavitation occurring there. It can be shown[7], however, that the width of the cavitation region, i.e., that region at the center of each annulus in which negative pressures would be generated but for the cut-off in Eq. (2), is approximately $\Delta(M_0/2)/(1 - M_0/2)$. And since Eq. (1) implies $M_0 << 1$, we are justified in neglecting this effect, at least for the present). Each of the fluid annuli will then begin dividing in half with the outer half moving outward and the inner half inward. The Lagrangian element defined within $R_a \leq r \leq R_b$ will collide with the element defined within $R_c \leq r \leq R_d$ in a time increment $t_1 - t_0 = \delta/2U_1 = \delta C_0/2\gamma_0 e_0$. These two fluid elements are shown shaded in Figure 1 for $t \geq t_0$; for clarity, the boundaries of the remaining fluid elements are identified with dashed lines. Maximum momentum interaction will be achieved if the collision occurs after pressure relief has been fully accomplished in each segment, i.e., if $t_1 - t_0 > t_0$. This inequality can be re-written as

$$\delta/\Delta > M_0 \tag{6}$$

Upon collision, shocks will reflect with speed S from the contact interface, which is a line of symmetry in the non-divergent case. The particle velocity and specific internal energy behind the shock then regain their initial values, i.e.,

$$U_2 = 0 \tag{7}$$

$$e_2 = e_0 \tag{8}$$

Restricting attention to the right-hand, or outward side of the contact interface, mass and momentum conservation require

$$\rho_1(S - U_1) = \rho_2 S \tag{9}$$

and

$$P_2 + \rho_2 S^2 = \rho_1(S - U_1)^2 \tag{10}$$

where due account has been taken of the fact that both P_1 and U_2 are zero.

Formal solution of (2), (9) and (10) yields

$$\eta_2 = A + \sqrt{A^2 - B} \tag{11}$$

$$\text{and} \quad -\eta_2 S/C_0 = P_2/P_0 = \eta_1\eta_2 M_0/(\eta_2 - \eta_1) \tag{12}$$

$$\text{where } A = \frac{1}{2}\left[(1 - M_0) + \eta_1(1 + M_0^2)\right] \tag{13}$$

$$\text{and} \quad B = \eta_1(1 - M_0) \tag{14}$$

η_1 represents the average density of the fluid elements at the moment of the collision (ahead of the shocks). In a linear field, this is readily determined by solving (2a) with $P_1(\eta_1, e_1) = 0$. The result is

$$(\eta_1)_{max} = 1 - M_0(1 - \gamma_0 M_0/2) \tag{15}$$

The subscript (max) is appended to signify that this is the maximum value η_1 can take if the pressure is to be everywhere zero before collision. We note

that $\eta_1 < (\eta_1)_{max}$ even for slab (linear) geometry if account is taken of the cavitation developed at the midpoint of each annulus by the reflected rarefaction fan - neglected here because of the assumption that $M_0 << 1$. That $\eta_1 < (\eta_1)_{max}$ for cylindrical or spherical flows is easy to demonstrate. In a divergent flow field the flow cross section for the radially outward-moving segment continues to increase and since the pressure is uniformly zero, there can be no compensating acceleration. Then, by continuity, the density must decrease in this segment. The EOS (2) is not symmetric about $(\eta_1)_{max}$, however, so the converging flow in the radially inward-moving segment will be accelerated with $\eta_1 \gtrsim (\eta_1)_{max}$ in this segment. At contact, the average density of the ensemble must then be less than the maximum and will be lower the greater is the initial separation distance, δ.

Now, since it is clear on physical grounds that

$$(\eta_1)_{max} \leq \eta_2 \leq 1 \tag{16}$$

equations (11) - (12) can be simplified somewhat by taking the cavitated Hugoniot to be approximately equal to the reference isochore, i.e., by setting

$$\eta_2 \cong 1 \tag{17}$$

so that

$$-S/C_0 = P_2/P_0 = \eta_1 M_0/(1 - \eta_1) \tag{18}$$

The relative error in the pressure is then

$$\varepsilon \equiv \left[(P_2)_{exact} - P_2\right] \Big/ (P_2)_{exact} = (\eta_1/\eta_2)\left[(1 - \eta_2)/(1 - \eta_1)\right] \qquad (19)$$

where $(P_2)_{exact}$ derives from (12).

ε is plotted as a function of η_1 in Figure 3 with η_2 evaluated from (11), (13) and (14), using $M_0 = 10^{-2}$. This is the approximate value of M_0 derived when the total neutronic energy deposition per unit length, at the horizontal plane passing through the equator of the fusion pellet, is averaged over the lithium fall mass per unit length - assuming a 1000 MW_e reactor with a lithium fall thickness of 1 m beginning at an inner radius of $\sim$0.5 m. It is seen in Figure 3 that the approximation (17) results in at most a 20% relative error in the calculation of the collision pressure. Even this result is somewhat misleading because the maximum relative error occurs when the pressure gradient $\partial P/\partial \eta_1$ is very steep. Figure 4, which plots the collision pressure as a function of the pre-collision density, shows that Eqs. (17)-(18) are indeed a very good approximation to the exact solution.

Figure 4 also shows that a very small decrease in the pre-collision density produces a very large decrease in the collision pressure. Cavitating the fluid by only 1% below $(\eta_1)_{max}$ ($\approx$ 0.99 for $M_0 = 10^{-2}$) decreases the shock pressure by almost 40%!

The physical picture may be clarified somewhat by the P-V diagram sketched in Figure 5 ($V = 1/\eta$). Point A corresponds to the initial state attained upon energy deposition, i.e., $P_A = P_0(V = 1, e = e_0)$. The fluid is then isentropically expanded along the path A $\rightarrow$ B $\rightarrow$ C. Point B corresponds to the "linear" geometry case, i.e., $P_B = P(\eta_1 = (\eta_1)_{max}, e = e_1)$. Collision occurs at point C. The path C $\rightarrow$ D is a Rayleigh line and no

intermediate states are possible. Conservation of energy requires that the area $\overline{AEBOD}$ equals $\overline{CDO}$; it is therefore clear that P_D, the collision pressure, rapidly decreases as V_C increases. The shaded area $\overline{CEF}$ represents the energy dissipated by the collision.

Now, once again referring to Figure 1, when the shocks have reached the Lagrangian surfaces, R_a and R_d, they are reflected as rarefactions behind which the particle speed will be

$$U_3 \approx P_2/\rho_2 C_0 \tag{20}$$

The net impulse eventually imparted to the wall is proportional to the total outward-directed momentum $\rho_0\Delta(U_1 + U_3)/2$. Had the energy been deposited in a single annular fall, without any imbedded void gaps, the outward-directed momentum would have been simply $\rho_0\Delta U_1$. Thus the impulse ratio is $(U_1 + U_3)/2U_1$ or, employing (3), (17), (18) and (20):

$$I/I_0 = \left[1 + M_0\eta_1/(1 - \eta_1)\right]/2 \tag{21}$$

If the colliding fluid masses are cavitated by only 1% below $(\eta_1)_{max}$, the impulse ratio for $M_0 = 10^{-2}$ is 0.75.

3.0 NUMERICAL EXPERIMENTS

Equations (18) and (21) predict the pressure and outward-directed momentum given η_1, the average density just prior to collision. For slab geometry and $M_0 << 1$, equation (15) provides a satisfactory estimate of this quantity. No such simple estimate is evident when the geometry is divergent because of the absence of symmetry about the radius of collision and the inhomogeneity of the colliding fluid packets. In general, η_1 in this case will depend on the geometry (inner annular radius, annular thickness and gap width) as well as on M_0. On the other hand, numerical solution of the initial value problem posed in Figure 1 by finite difference methods is quite straightforward. Figure 6 depicts the results of a number of such calculations made with the AFTON code[7]. The impulse ratio, I/I_0, is plotted as a function of the ratio of the gap width to thickness ratio, δ/Δ. Two different initial energy deposition functions were used, a "typical" distribution and a uniform distribution. In the former, e_0 varied from $\sim$ 2 MJ/kg at the inner radius (0.5 m in all cases) to $\sim 2 \times 10^{-2}$ MJ/kg at the outer. In the latter, e_0 was constant throughout the fall and equal to the mass-averaged energy derived from the non-uniform case (0.225 MJ/kg, corresponding to $M_0 = 10^{-2}$). For both deposition functions, calculations were first made for a single annular fall ($\delta/\Delta = 0$). The total outward-directed momentum for the non-uniform deposition was 42% higher than for the uniform case (the peak outward velocity, at the outer radius, was almost 5 times higher). The ordinate values for the points shown in Figure 6 (open for uniform deposition and shaded for non-uniform) were derived by dividing the total outward-directed momentum obtained with the fall initially

split (into n + 1 annuli separated by n void gaps; n = 1,9) by the total outward-directed momentum for the single annular geometry and the same initial energy distribution and total mass. The multi-annulus problems were generated from the single annulus problem after the energy was deposited. This was done, for n gaps, by dividing the single annulus into n + 1 Lagrangian segments and inserting the gaps of desired thickness, beginning with the innermost gap and proceeding outward. After each gap was inserted, the thickness of all succeeding segments (and the mesh spacing by which they were delineated) was appropriately foreshortened to conserve mass.

Considering first the single gap calculations, it is remarkable that although the impulse depends very much on the initial spacial energy distribution, the impulse ratio is effected very little, if at all, it's value being determined strictly by the mass-averaged energy (represented by M_0) and the geometry. Using the numerical data derived from the calculations at $M_0 = 10^{-2}$, we found that a very good fit was obtained with the empirical expression

$$I/I_0 = \left\{1 + 1/[1 + (\delta/\Delta)/4M_0]\right\}/2 \qquad (22)$$

as evidenced in Figure 6. To test the M_0 dependence, we increased this parameter by an order of magnitude, to 10^{-1}, and used the code to calculate I_0 (single annular fall) and I (1 void gap, $\delta/\Delta = 0.25$); the ratio I/I_0 so determined was 0.801. This agrees with the value of 0.808 predicted by (22) to within better than 1%.

If (21) and (22) are equated, it is possible to "experimentally" deduce the parameter η_1 for the single gap case:

$$(\eta_1)_{R_0=0.5m} = [1 + M_0 + (\delta/\Delta)/4]^{-1} \qquad (23)$$

For $\delta/\Delta \to 0$, $\eta_1 \to (1 + M_0)^{-1} \approx 1 - M_0$ for $M_0 << 1$, which is the correct density ratio in this limit.

Figure 6 also shows the effect of gap thickness on the impulse ratio when the number of gaps is increased. A much smaller relative gap spacing is required to effect a given impulse reduction when the number of gaps is increased from 1 to 9. Also, very little is to be gained by increasing the void to annulus thickness ratio above 0.25 when $M_0 = 10^{-2}$. Figure 7, which crossplots Figure 6, shows moreover that little is to be gained by splitting the fall into more than 10 or so concentric annular segments.

3.1 A PRACTICAL EXAMPLE: MULTI-ANNULAR FALL DISASSEMBLY IN AN ICF REACTOR

Figure 8 shows the calculated mass-averaged outward-directed velocity, $\bar{U}$, as a function of time for two different fall designs in a HYLIFE reactor[2,5]; the ordinate was obtained by dividing the total outward-directed momentum by the outward-moving fluid mass. In the design labeled "actual", 300 jets, each of 200 mm diameter and arrayed around the DT pellet in a close-packed annular fashion, were simulated by 9 concentric annuli separated by void gaps. The innermost annulus was located at a radius of 0.5 m and was associated with the first 12 jets so that it contained 4% of the total jet mass. The second annulus had 6% of the mass, the third 8%, etc.

up until the eighth, which had 18%, and each of these was separated by a void gap of 118 mm. The outermost annulus contained the remaining 12% of the mass and was located 88 mm from it's inner neighbor.

For $t \leq 60$ μs, the problem is dominated by x-ray deposition and ionic debris from the DT pellet, which penetrate only a very thin layer in the innermost exposed jets (inner annulus). The details of the resulting implosion and blowback have been discussed elsewhere[9]. In brief, a hot, high-pressure lithium plasma is created in the core which then expands, against the jets, flows around or in between them, and continues to expand until contact is made with the first wall - located 2 or more meters beyond the last row of jets. Coupled with the jet disassembly induced by x-ray spall and neutron heating, this results in a complicated three-dimensional flow. A quasi-one-dimensional method was, however, devised to calculate a first approximation of the drag impulse exerted on the jet array by the venting plasma[2]. This impulse, which was effectively terminated by $t \approx 350$ μs, was then superimposed on the radial motion of the concentric annuli caused by the isochoric heating. The object, of course, was to obtain a reasonable estimate of the impulse imparted to the first wall by the lithium.

For the "actual" design, the spacial distribution of particle velocity and density is shown in Figure 9 at $t = 60$ μs, when the plasma first arrived at the innermost annulus. An Eulerian inner boundary was imposed at $r = 0.5$ m, since the cavity region had been calculated separately to determine the blowback and crossflow. All other annular boundaries were Lagrangian until gap closure was attained, after which a gradual, accordion-like[8] rezone was employed. It can be seen that at 60 μs, the fast-moving x-ray spall layer from the first "row" has already made contact with the second row. The peak

outward-directed velocity at this time exceeds 2 km/s. Also noteworthy in Figure 9 is the splitting evidenced in the remaining annuli by the non-uniform neutron heating (the fluid density is shown by the shaded overlay; the reference liquid density was 0.518 g/cc).

By t = 1 ms, Figure 8 shows that the average outward-directed velocity has decreased to about 52 m/s. Figure 10 illustrates the velocity and density distribution. Contact has been made by all but the last three annuli. By t = 5 ms, $\bar{U}$ in Figure 8 has dropped to its minimum value of 36 m/s and Figure 11 shows that all of the fluid annuli have joined. The outward-moving fluid has begun to compact, a process that is essentially completed 10 ms later as seen in Figure 12. At this point, virtually the entire fluid mass (at the plane of the DT pellet) is at near-liquid density and is moving outward at a uniform velocity of 38 m/s.

3.2 NUMERICAL ERROR

Most practical schemes for the solution of arbitrary initial value problems in continuum mechanics are dispersive, i.e., if the solution is thought of as being expanded in Fourier series (with time dependent coefficients), different components travel with different speeds. In particular, components whose wavelengths are of the same order as the spacial mesh discretization interval are always falsified somewhat. In most cases this is of little interest as long as the amplitude of the falsified components remains small everywhere, a condition that is usually easy to meet with a judicious choice of artificial viscosity and timestep. Unfortunately, however, dispersion may lead to serious error in the isochoric heating

problem. The reason is that the small decreases in the average density that result when square corners are rounded or smeared can cause large decreases in the collision pressure (cf. Figure 4). In numerical experiments performed with just two colliding slabs (linear geometry) and with $M_0 << 1$, so that the actual dissipation must be negligible, upwards of 500 zones were required to assure this result. And while the calculation described in Figures 9-12 did employ 500 zones, there were many more free surfaces and collisions. Moreover, of the 500 zones initially employed, only about 300 ended up delineating the liquid and two-phase liquid-vapor region, the other 200 having blown off early (within the first few microseconds) with the plasma into the core cavity.

There has been some recent progress with the development of numerical methods that are (practically) non-dispersive[10,11]; Keith Miller's moving finite element (MFE) method[11] appears to be especially promising in this regard. They have not yet been adapted to problems as complex as those under consideration here. Alternately, the magnitude of the error induced by dispersion with the present algorithm might be determined by minimizing the gap width between annuli. Figure 6 shows that if the gap width is of the order of M_0, in accord with the inequality (6), the dissipation is very much reduced, without effecting the desirable spacial averaging of momentum. Accordingly, a multi-annular fall geometry was set up with the same mass and energy distribution as for the actual design described above, but with the much reduced gap spacing. The performance of this "minimum gap" design is shown in Figure 8. With the gap spacing reduced such that the first collisions occur everywhere near simultaneously, and in a time period not much exceeding the time for initial pressure relief, the average outward-directed

velocity is determined much more rapidly than with the actual design. The minimum value of $\bar{U}$ of 31.5 m/s occurs at about 300 μs and by 1 ms, the available potential energy of collision has been reconverted to kinetic energy and $\bar{U}$ has stabilized at 41.5 m/s. This may be directly compared with the 38 m/s obtained with the actual design, since the identical crossflow impulse was superimposed on both problems. The 10% difference is probably an acceptable margin of error, considering the rather crude model.

4.0 IMPACT ON THE FIRST WALL

Our main concern is that the hoop stress that results from fluid impact does not exceed the maximum allowable working stress. If the first wall were located at 2.3 m, i.e., directly behind the nearly compacted fluid packet in Figure 12, the impact pressure would be $P_3 \approx \rho_0 \bar{U} C_0$. For lithium, $\rho_0 = 0.518$ g/cc, $C_0 = 4.5$ km/s, and if we conservatively take $\bar{U} = 41.5$ m/s, $P_3 = 96.7$ MPa. This pressure will persist for a duration $\tau = 2\ell/C_0$, where ℓ is the thickness of the fluid packet (from Figure 12, $\ell \approx 2.3 - 1.8 = 0.5$ m), so that $\tau \approx 0.22$ ms. The natural period of the wall is $T = 2\pi R_w \sqrt{E_w/\rho_w}$, where R_w is the wall radius, E_w is the Young's modulus and ρ_w is the density. If 316 stainless steel is used, and with $R_w = 2.3$ m, $T = 2.85$ ms so that $\tau/T << 1$. In this case, it has previously been shown[1] that the peak hoop stress, $\sigma_{max} = (P_3\tau/\delta_w)\sqrt{E_w/\rho_w}$, where δ_w is the wall thickness. Assuming $\delta_w = 100$ mm, the peak hoop stress under these conditions would be 1.08 GPa, at least 10 times the recommended working stress for 316 SS under fusion reactor conditions[1].

Now suppose the first wall is relocated at a 5 m radius. Since the pressure in the outward-moving fluid packet in Figure 12 is everywhere zero, no further acceleration is possible and the packet will coast at the speed $\bar{U}$ until impact. The speed is uniform throughout so the thickness of the fluid packet will be maintained. But continuity requires that as the field diverges, the density must drop. If the density is $\approx \rho_0$ at t = 15 ms, impact will occur at 15 + (5-2.3)/.0415 = 80 ms at which time the density ratio will be $\eta = \rho/\rho_0 = (2.3^2 - 1.8^2)/(5^2 - 4.5^2) = 0.43$. Physically, we expect that cavities will be initially formed within the bulk

liquid. If η is sufficiently small, the fluid will appear as a rain of drops or fragments but this is probably not the case here. The impact of the cavitated liquid on the (assumed rigid) wall is exactly analogous to the symmetrical impact described by (18). Within the present context, $P_3 = \rho_0 \bar{U}^2 \eta/(1-\eta)$; with $\eta = 0.43$ the impact pressure $P_3 = 0.67$ MPa, more than 100 times less than obtained when R_w was 2.3 m, but still $2/(1 - \eta)$ or 3.5 times the Bernoulli pressure. Also from (18), the compaction speed, S, will be $\bar{U}\eta/(1-\eta) = 31.3$ m/s, so that in this case the pressure will persist for a period $\tau \approx \ell/S + \ell/C_0 \approx \ell/S = 16$ ms. And if $R_w = 5$m, $T = 6.2$ ms and $\tau/T > 1$. In this case, the peak hoop stress is simply $\sigma_{max} = 2P_3R_w/\delta_w = 67$ MPa, within the allowable range.

5.0 SUMMARY AND CONCLUSIONS

Steep velocity gradients can be produced in a liquid slab if it is suddenly and non-uniformly heated. These gradients can be effectively smeared out if the slab is subdivided into a number of slabs that are separated by gaps. The gaps allow pressure relief from surfaces interior to the main inner and outer boundaries, which promotes momentum exchange between fluid elements traveling in opposite directions, thereby averaging out the velocity distribution. This effect is very important in an ICF reactor because even if the impulse delivered to the wall is within tolerable limits, the bombardment by high-velocity spall fragments can eventually cause severe erosion damage.

If instead of slabs, concentric liquid rings are considered, the impulse itself can be reduced. The inability of liquids to support tensile stresses results in the formation of incipient cavities in the outward-moving segments of each ring. On contact with the inward-moving segments, shock compression of the "porous" liquid causes energy to be dissipated and the collision pressure can be very much less than in the equivalent slab impact. The rebound velocity varies directly with this pressure so that an inelastic collision results and the outward-directed momentum (which forms the impulse imparted to the first wall) is reduced.

A simple model was developed for predicting the pressure developed when cavitated liquid masses collide with each other or with a rigid wall. The pressure was found to be a strong function of the pre-collision density; cavitating lithium by only 1% results in a 40% reduction in the impact pressure for an impact Mach number of 10^{-2}. A direct result of this effect is that numerical dispersion can introduce significant error when calculating

the disassembly and subsequent interaction of pressurized liquids with conventional finite difference or finite element methods. Finer mesh discretization is the (costly) remedy employed here but it would be better to use methods that eliminate dispersion altogether, if these can be found.

Numerical simulations were made of the response of a multi-annular lithium fall in a 1000 MW_e reactor to the energy deposition from the fusion pellet. The resultant impact load on the first wall of the reactor was found to depend very much on its location. Placed at a radius of 2.3 m, in contact with near-normal density liquid, the peak hoop stress exceeded 1 GPa. Placed at a 5 m radius, as in the actual design, so that the average density at contact was more than halved, the peak hoop stress was reduced by a factor of 16 to an acceptable level.

NOTICE

"This report was prepared as an account of work sponsored by the United States Government. Neither the United States nor the United States Department of Energy, nor any of their employees, nor any of their contractors, subcontractors, or their employees, makes any warranty, express or implied, or assumes any legal liability or responsibility for the accuracy, completeness or usefulness of any information, apparatus, product or process disclosed, or represents that its use would not infringe privately-owned rights."

Reference to a company or product name does not imply approval or recommendation of the product by the University of California or the U.S. Department of Energy to the exclusion of others that may be suitable.

REFERENCES

1. L. A. Glenn and D. A. Young, Nucl. Engrg. Des., 54, (1979) 1-16.
2. L. A. Glenn, Lawrence Livermore Laboratory Report UCRL-83051 (1979) accepted for publication in Nucl. Engrg. Des.
3. E. F. Plechaty, D. E. Cullen, R. J. Howerton and J. R. Kimlinger, Lawrence Livermore Laboratory Report UCRL-50400, Vol. 16, Rev. 2 (1978).
4. W. R. Meier and W. B. Thomson, Lawrence Livermore Laboratory Report UCRL-80782 (1978), presented at Third ANS Topical Meeting on Fusion, May 9-11, 1978, Santa Fe, NM.
5. L. A. Glenn, Cavity Dynamics in the HYLIFE Inertial Confinement Fusion Reactor, 1980 Topical Meeting on Inertial Confinement Fusion, February 26-28, 1980, San Diego, CA.
6. Y. B. Zel'dovich and Y. P. Raizer, Physics of Shock Waves and High-Temperature Hydrodynamic Phenomena, v. II, Academic Press (1967) 712-716.
7. L. A. Glenn, J. Appl. Math. Phys. (ZAMP), 25 (1974) 383-398.
8. L. A. Glenn, Lawrence Livermore Laboratory Report UCRL-52512 (1978).
9. L. A. Glenn, The Influence of Radiation Transport on Lithium Fall Motion in an ICFR, to appear.
10. A. J. Chorin, J. Comp. Phys. 25 (1977) 253-272.
11. R. J. Gelinas, S. K. Doss and K. Miller, Science Applications Inc. Report No. SAI/PL/F179 (1979).

LIST OF FIGURES

1. Two concentric liquid rings separated by a void gap; suddenly heated at $t = 0$; at $t = t_0$, when the pressure has just released; and at $t \geq t_1$, when collision occurs.
2. Spacial distribution of particle velocity at $t = t_0$, when the pressure has just released (slab geometry).
3. Relative error in computing the pressure by assuming the Hugoniot to be approximated by the reference isochore.
4. Collision pressure as a function of pre-collision density.
5. Disassembly and collision sketched in the pressure-specific volume plane.
6. Impulse imparted to the wall as a function of gap-to-annulus thickness ratio. Numerical results computed for 1 and 9 gaps, and for uniform and non-uniform spacial energy deposition (refer to the text for details).
7. Impulse imparted to the wall as a function of the gap number for different gap-to-annulus thickness ratios and an impact Mach number of 10^{-2} (crossplot of the data in Figure 6).
8. Calculated mass-averaged outward-directed fall velocity as a function of time for two different fall designs in a 1000 MW_e ICF reactor (refer to the text for details).
9. Spacial distribution of particle velocity and density (shaded) for the "actual" design of Figure 8 at $t = 60$ μs.
10. Spacial distribution of particle velocity and density (shaded) for the "actual" design of Figure 8 at $t = 1$ ms.
11. Spacial distribution of particle velocity and density (shaded) for the "actual" design of Figure 8 at $t = 5$ ms.
12. Spacial distribution of particle velocity and density (shaded) for the "actual" design of Figure 8 at $t = 15$ ms.

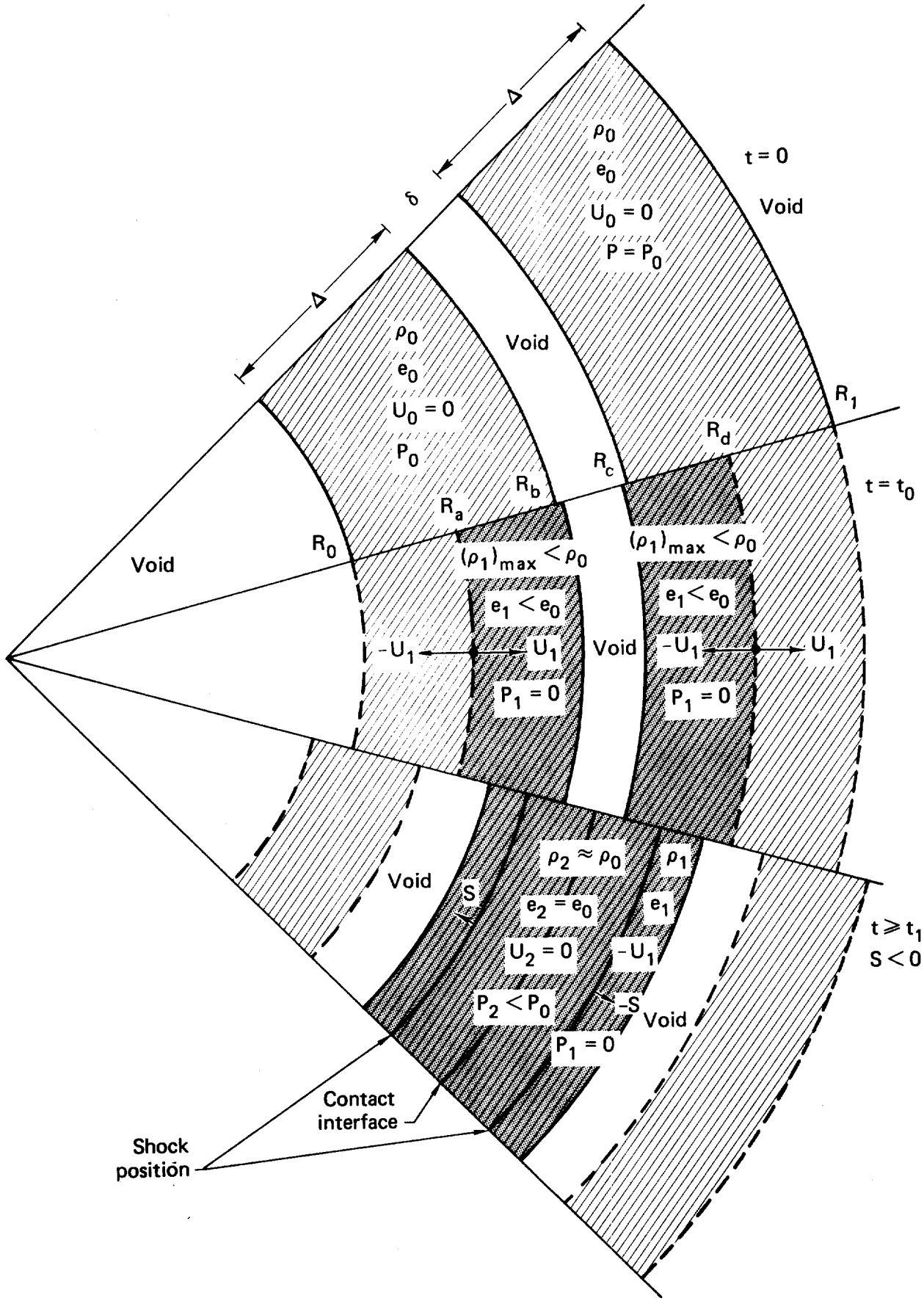
Δ
δ
Δ
ρ_0
e_0
$U_0 = 0$
$P = P_0$
t = 0
Void
Void
ρ_0
e_0
$U_0 = 0$
P_0
R_1
R_d
R_c
R_b
R_a
R_0
$t = t_0$
Void
$(\rho_1)_{max} < \rho_0$
$(\rho_1)_{max} < \rho_0$
$e_1 < e_0$
$e_1 < e_0$
$-U_1$
U_1
Void
$-U_1$
U_1
$P_1 = 0$
$P_1 = 0$
Void
$\rho_2 \approx \rho_0$
ρ_1
S
$e_2 = e_0$
e_1
$t \geq t_1$
$S < 0$
$U_2 = 0$
$-U_1$
$P_2 < P_0$
$-S$
Void
$P_1 = 0$
Contact interface
Shock position

FIGURE 1

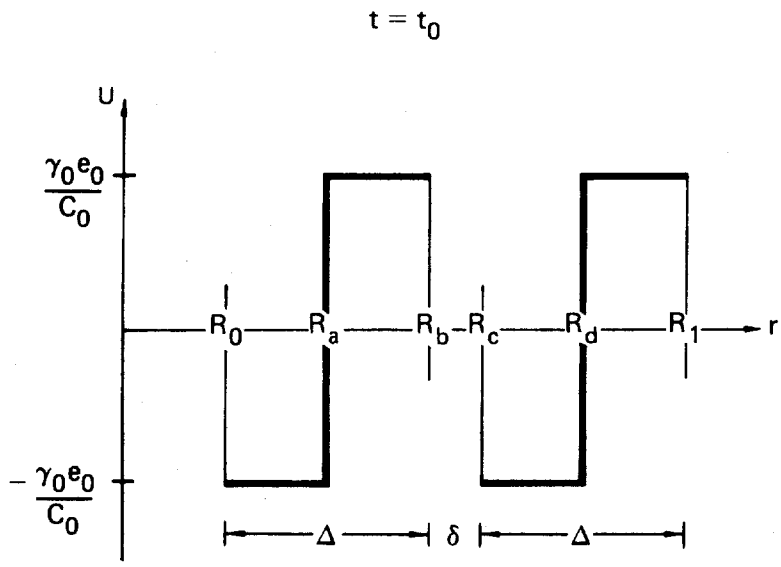

FIGURE 2

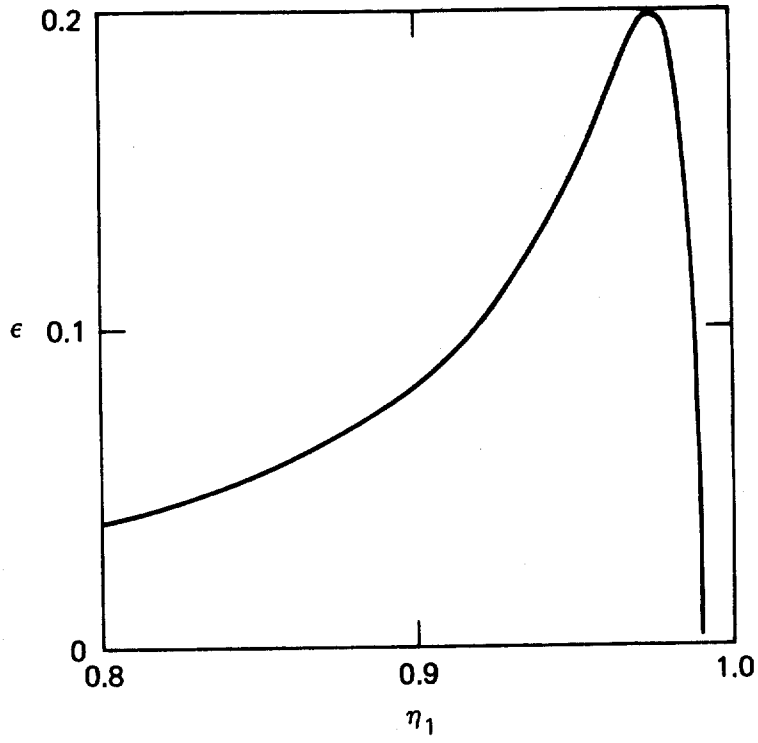

FIGURE 3

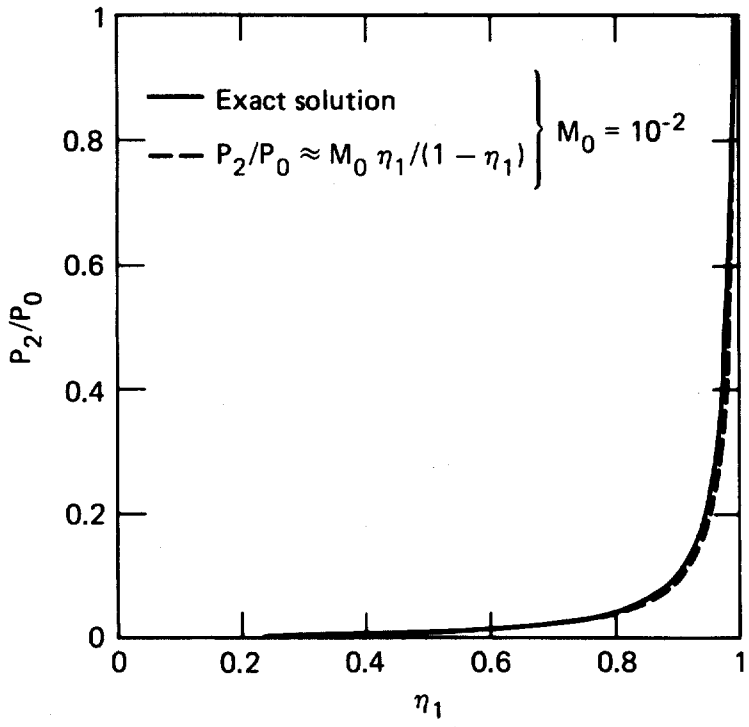
Exact solution
$P_2/P_0 \approx M_0\,\eta_1/(1-\eta_1)$
$M_0 = 10^{-2}$
P_2/P_0
η_1
0
0.2
0.4
0.6
0.8
1

FIGURE 4

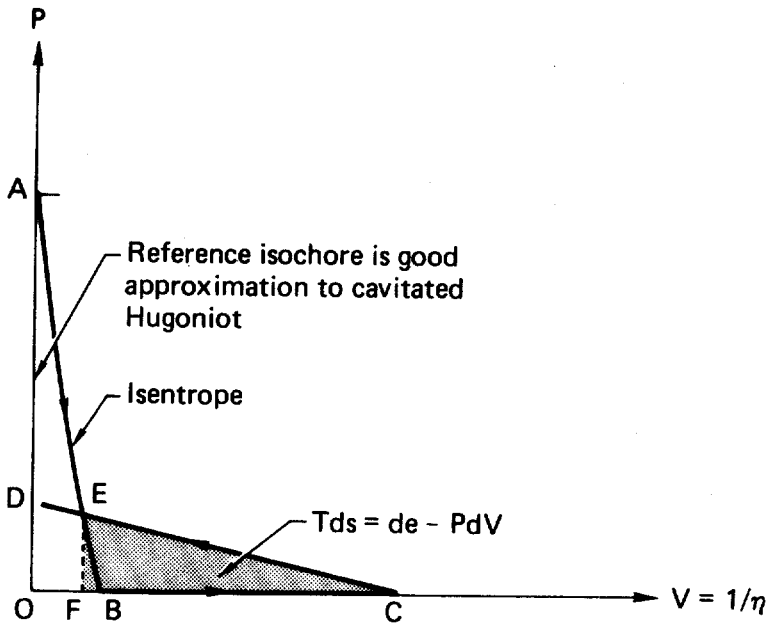
P
A
Reference isochore is good approximation to cavitated Hugoniot
Isentrope
D
E
Tds = de - PdV
O
F
B
C
V = 1/η

FIGURE 5

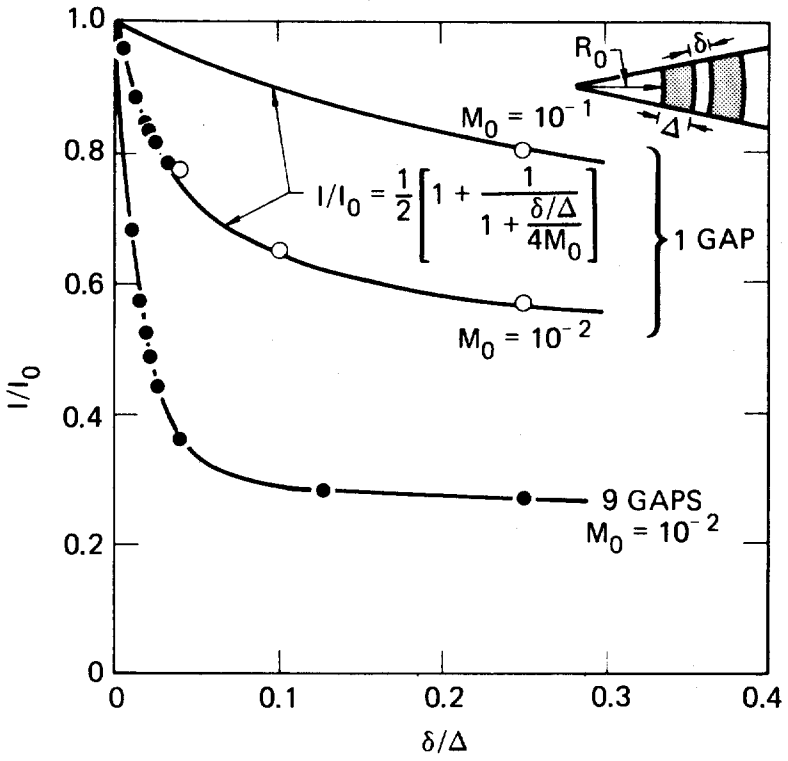
1.0
0.8
0.6
0.4
0.2
0
0
0.1
0.2
0.3
0.4
I/I0
δ/Δ
R0
δ
Δ
M0 = 10-1
I/I0 = 1/2 [1 + 1/(1 + δ/Δ / 4M0)]
1 GAP
M0 = 10-2
9 GAPS
M0 = 10-2

FIGURE 6

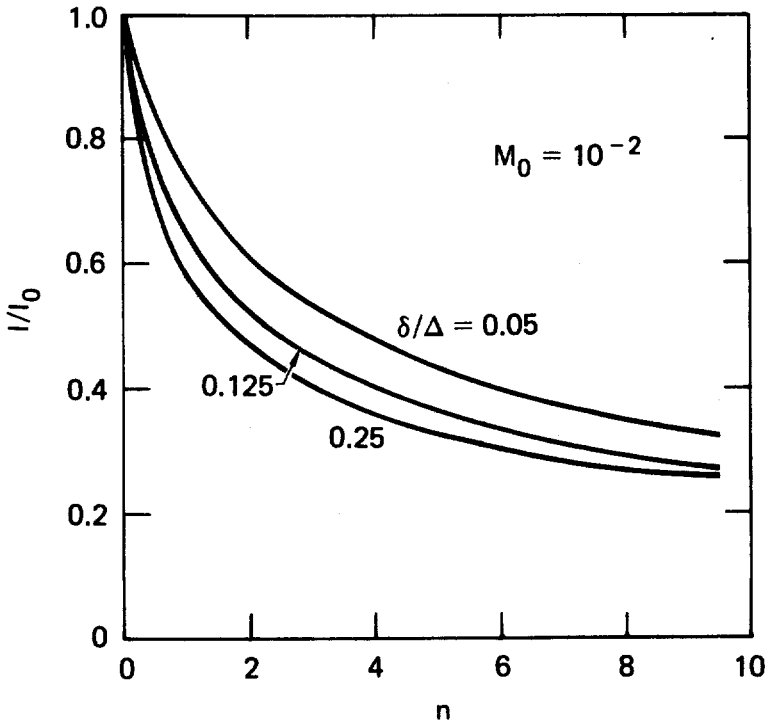

FIGURE 7

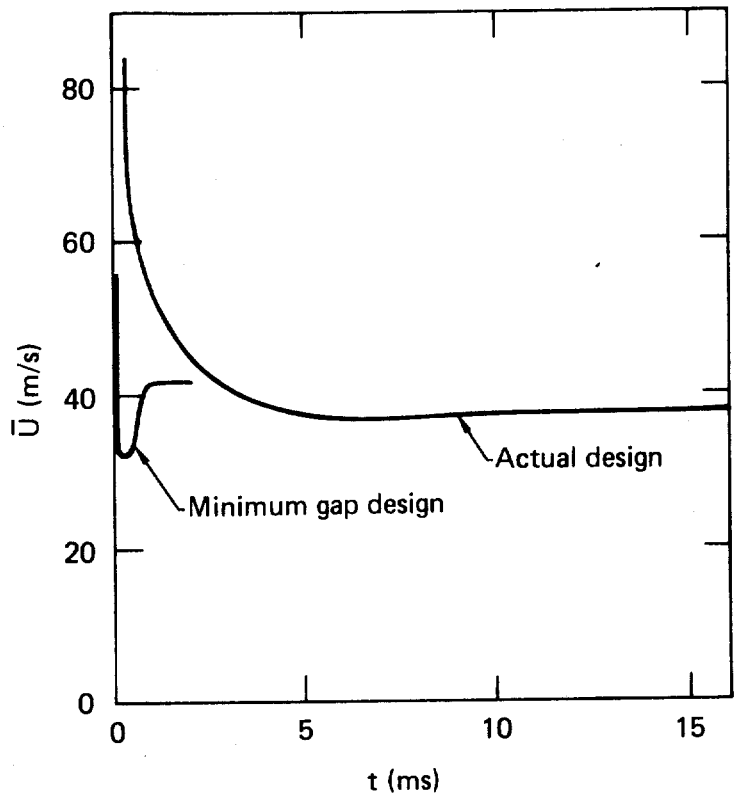
80
60
40
20
0
$\bar{U}$ (m/s)
0
5
10
15
t (ms)
Actual design
Minimum gap design

FIGURE 8

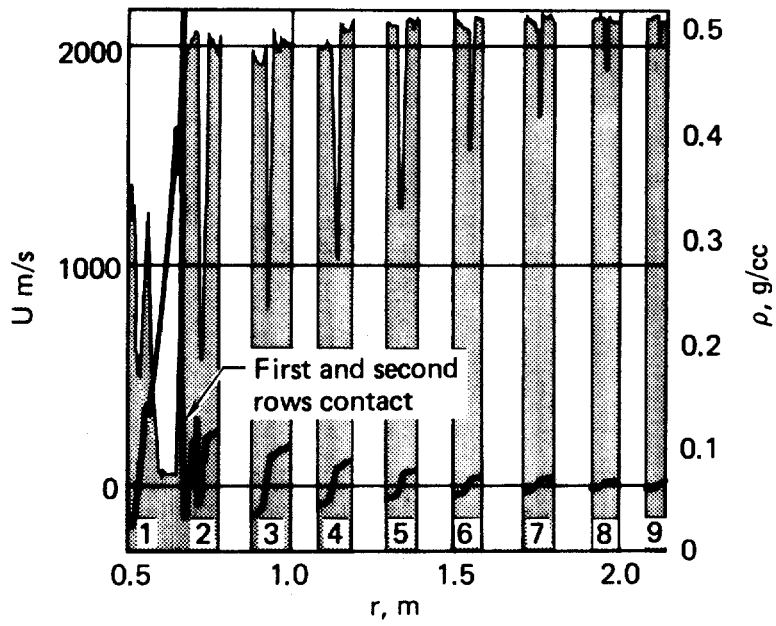
2000
1000
0
U m/s
0.5
0.4
0.3
0.2
0.1
0
ρ, g/cc
First and second
rows contact
1
2
3
4
5
6
7
8
9
0.5
1.0
1.5
2.0
r, m

FIGURE 9

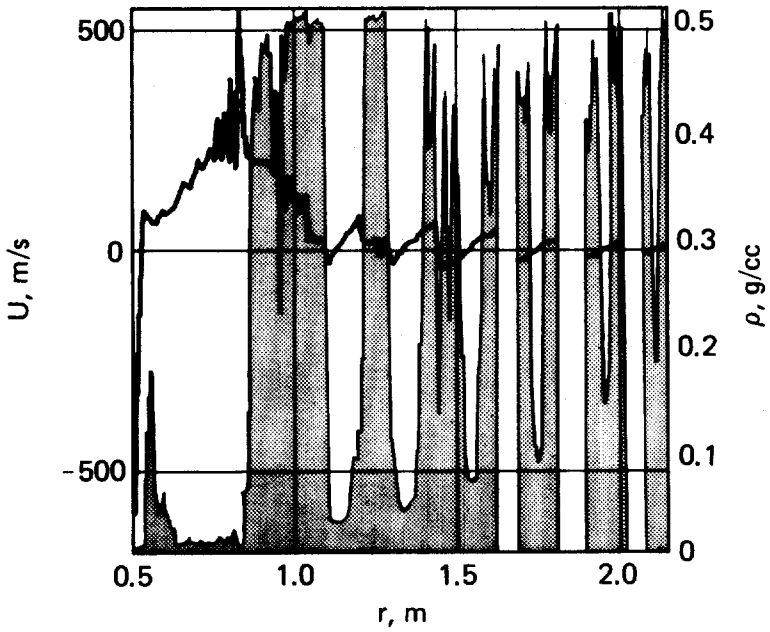

FIGURE 10

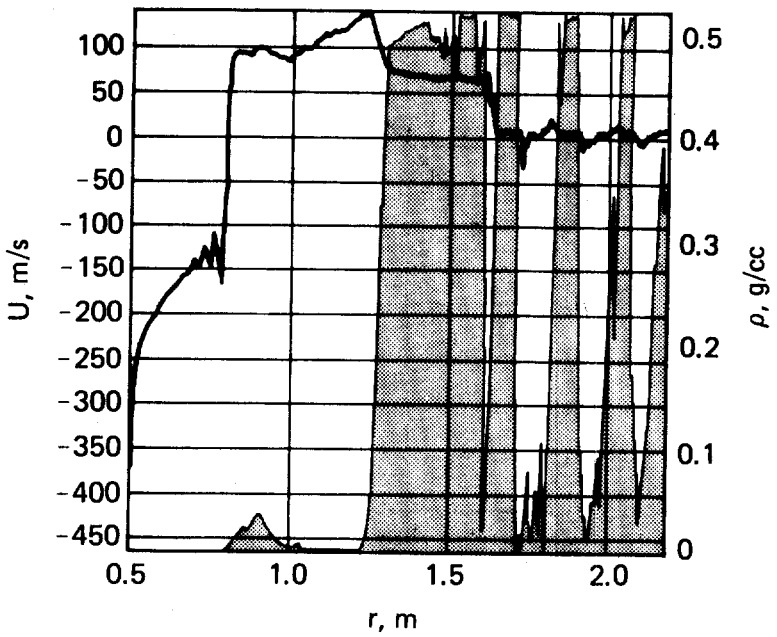
100
50
0
-50
-100
-150
-200
-250
-300
-350
-400
-450
U, m/s
0.5
0.4
0.3
0.2
0.1
0
ρ, g/cc
0.5
1.0
1.5
2.0
r, m

FIGURE 11

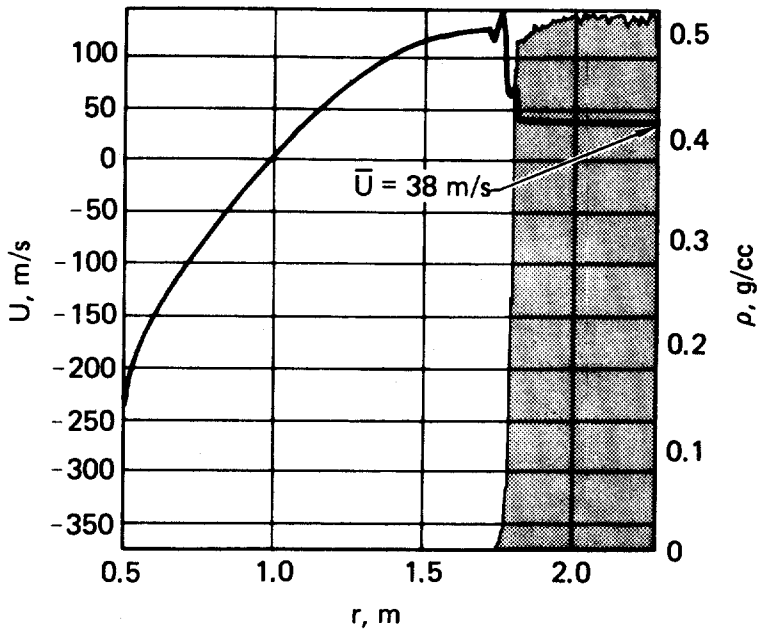
100
50
0
-50
-100
-150
-200
-250
-300
-350
U, m/s
0.5
1.0
1.5
2.0
r, m
0.5
0.4
0.3
0.2
0.1
0
ρ, g/cc
Ū = 38 m/s

FIGURE 12